HHS Public Access

Author manuscript

J Mol Cell Cardiol. Author manuscript; available in PMC 2020 August 01.

Published in final edited form as:

J Mol Cell Cardiol. 2019 August ; 133: 199–208. doi:10.1016/j.yjmcc.2019.06.013.

Phenotyping an adult zebrafish *lamp2* cardiomyopathy model identifies mTOR inhibition as a candidate therapy

Alexey V. Dvornikov[1,+], **Mingmin Wang**[1,2], **Jingchun Yang**[1,#], **Ping Zhu**[1], **Tai Le**[3], **Xueying Lin**[1], **Hung Cao**[3,4], **Xiaolei Xu**[1,*]

[1]Department of Biochemistry and Molecular Biology, Department of Cardiovascular Medicine, Mayo Clinic, Rochester, Minnesota, USA

[2]Dongzhimen Hospital, Beijing University of Chinese Medicine, Beijing, China

[3]Department of Electrical Engineering and Computer Science, University of California Irvine, California, USA

[4]Department of Biomedical Engineering, University of California Irvine, California, USA

Abstract

Adult zebrafish is an emerging vertebrate model for studying genetic basis of cardiomyopathies; but whether the simple fish heart can model essential features of hypertrophic cardiomyopathy (HCM) remained unknown. Here, we report a comprehensive phenotyping of a *lamp2* knockout (KO) mutant. *LAMP2* encodes a lysosomal protein and is a causative gene of Danon disease that is characterized by HCM and massive autophagic vacuoles accumulation in the tissues. There is no effective therapy yet to treat this most lethal cardiomyopathy in the young. First, we did find the autophagic vacuoles accumulation in cardiac tissues from *lamp2* KO. Next, through employing a set of emerging phenotyping tools, we revealed heart failure phenotypes in the *lamp2* KO mutants, including decreased ventricular ejection fraction, reduced physical exercise capacity, blunted β-adrenergic contractile response, and enlarged atrium. We also noted changes of the following indices suggesting cardiac hypertrophic remodeling in *lamp2* KO: a rounded heart shape, increased end-systolic ventricular volume and density of ventricular myocardium, elevated actomyosin activation kinetics together with increased maximal isometric tension at the level of cardiac myofibrils. Lastly, we assessed the function of lysosomal-localized mTOR on the *lamp2*-associated Danon disease. We found that haploinsufficiency of *mtor* was able to normalize some characteristics of the *lamp2* KO, including ejection fraction, β-adrenergic response, and the

[*]Corresponding Author. Department of Biochemistry and Molecular Biology, Department of Cardiovascular Medicine, Mayo Clinic, 200 First Street SW, Rochester, Minnesota, 55905, USA. Phone: +1(507)2840685; xu.xiaolei@mayo.edu.
[#]Current address: Gastroenterology Research, Mayo Clinic, Rochester, Minnesota, USA
[+]Current address: Department of Cellular and Molecular Medicine, University of Arizona, Tucson AZ

Author contribution

A.V.D., J.Y., X.X. designed experiments, A.V.D., M.W, J.Y., P.Z, M.W., X.L. performed experiments and analyzed data, T.L. and H.C. performed ECG analysis. A.V.D. wrote a manuscript, X.X., H.C., X.L. edited the manuscript.

Disclosures

Nothing to disclose.

actomyosin activation kinetics. In summary, we demonstrate the feasibility of modeling the inherited HCM in the adult zebrafish, which can be used to develop potential therapies.

Keywords

cardiomyopathy; zebrafish; Danon disease; disease modeling; hypertrophic remodeling; cardiac contractility; single myofibril; mTOR

1. Introduction

About 1% of patients with hypertrophic cardiomyopathy (HCM) carry mutations in the lysosome-associated membrane protein 2 (*LAMP2*) gene [1, 2]. First described by M.J. Danon [3], these patients also manifest mild non-cardiac symptoms [4, 5] such as skeletal peripheral myopathy, mental retardation, hepatic involvement, and retinopathy [6]. This is the most lethal cardiomyopathy in the young and no effective therapy is yet available. Together with the *PRKAG2*--associated glycogen-storage disease and Anderson-Fabry disease, Danon disease was recognized as one of the three metabolic causes of HCM [7]. While the majority of inherited HCM are caused by mutations in sarcomeric genes [8], and there is mounting evidence for myofibrillar hypercontractility in sarcomere-based HCMs [9], how sarcomere contractility is affected in metabolic HCMs as a sequential pathological event has not been well defined.

LAMP2 is a type I integral membrane protein that is localized to lysosomes and late endosomes [10]. The *LAMP2* genome locus encodes three isoforms that share common N-terminal domains but have different C-terminus due to alternative splicing of the exon 9 [10]. While LAMP2A is a major component of chaperone-mediated autophagy, LAMP2B is required for macroautophagy [11]; and LAMP2C is restricted to the degradation of nucleic acids [12]. Mutations in *LAMP2* linked to Danon disease are mainly located in the region coding N-terminal part of the protein affecting all three isoforms [4, 13, 14]. Both mouse and iPSC models of Danon disease have been established [15, 16]. Similar to patients with Danon disease [10], these models manifest increased levels of the microtubule associated 1A/1B light chain-3 (LC3II) and a massive subcellular accumulation of autophagic vacuoles, suggesting dysregulated macroautophagy. Because these metabolic abnormalities must be the primary damage incurred by Lamp2 deficiency that sequentially leads to cardiac dysfunction, it is plausible that repairing metabolic abnormalities could be a therapeutic avenue. Mammalian target of rapamycin (mTOR) plays an important role in sensing nutrient and regulating metabolic processes such as macroautophagy [17, 18]. Upon fasting, mTOR is recruited to the surface of lysosome where LAMP2 is localized [19]. mTOR inhibition has been reported to be therapeutic for several types of cardiomyopathies including pressure and volume overload and isoproterenol induced, ischemic CMs, genetic ones linked to mutations in lamin A/C, and mouse model of LEOPARD syndrome [1, 20, 21]. Whether mTOR can be manipulated to repair metabolic abnormalities in the *LAMP2* mutants and/or to attenuate Danon disease remains untested.

The zebrafish has emerged as a new vertebrate model for studying cardiomyopathies [22–24]. Acquired cardiomyopathy models induced by anemia, doxorubicin, or isoproterenol

have been established, underscoring the conservation of cardiac remodeling in this species [25–28]. The majority of the causative genes linked to human dilated CM have their corresponding homologs in the zebrafish, supporting molecular conservation [23]. One of the key reasons for integrating the zebrafish model into cardiomyopathy studies is its powerful forward genetics. A mutagenesis screen-based strategy has been established in our laboratory enabling rapid identification of novel genetic factors and therapeutic targets [25]. Using a zebrafish *mtor* mutant that was identified from such a screen, we found that mTOR inhibition exerts therapeutic effects on both anemia and doxorubicin-induced cardiomyopathies [24, 25, 29, 30].

Partially due to the small size of the zebrafish heart and its unique sponge-like structure, cardiac phenotypes in adult zebrafish models of cardiomyopathy are poorly defined. For example, it remained to be established which phenotypic traits define HCM in the adult zebrafish. The past several years have witnessed the development of novel cardiac phenotyping tools in the zebrafish, including high frequency echocardiography [31], a Langendorff-like perfusion system [32], zebrafish electrocardiography [33–35], and biophysical methods to study cardiac contractile function at the level of myofibrils [36]. Here, we deployed these tools for detailed phenotyping of a *lamp2* knock out (KO) zebrafish and for assessment of the impacts of the mTOR inhibition. We were able to unveil HCM-like phenotypes in this zebrafish model of Danon disease as well as a therapeutic effect of mTOR inhibition in alleviating cardiac dysfunction.

2. Methods (See also: Online Supplement)

2.1 Fish husbandry

Zebrafish were handled under the guidelines of the Mayo Clinic Institutional Animal Care and Use Committee (IACUC protocol # is A00003513-18). WIK was used as a wild type strain. The fish were maintained at 28°C under the 14 hours light - 10 hours dark cycle.

2.2 Generation of lamp2^{e2} via TALEN

To generate *lamp2*^{e2} mutants, we injected one-cell stage WIK embryos with TALEN RNA . TALEN pairs were designed using Zifit (http://zifit.partners.org/ZiFiT/ChoiceMenu.aspx) and assembled using a Golden Gate Kit (Addgene). See Supplementary Data for details.

2.3 Ex vivo cardiac pump function assay

Our method was described in detail previously [32]. Briefly, hearts were excised from anaesthetized by tricaine (0.16 mg/ml in ice-cold water) 10-months-old fish of both sexes and tied to the tip of 34G blunt catheter for perfusion. We analyzed 15 hearts from WT, 16 hearts from LM group, and 11 hearts from LMT group. These numbers already excluded hearts with the visible damages of the ventricle or outflow tract during surgery. Then, during analysis, we excluded 3 hearts in WT and 3 hearts in LM groups for ex vivo functional parameter assessments (final N=12, 13 and 11 for WT, LM, and LMT groups, respectively). Exclusion criteria were the following: 1) a shallow increase in EDV with the linear increase in a flowrate (from 0.05 to 0.8 ml/min) suggesting leakage, 2) quick drop of ejection fraction

values <30% at the higher flowrates due to invisible damages. See Supplementary Data for details.

2.4. Quantification of atrial volume

We employed the same setup as we used for Langendorff-like heart perfusion. Instead of inserting a catheter via atrioventricular orifice, we inserted the cannula via outflow tract to introduce retrograde flow. We averaged areas obtained from these two perpendicular planes and normalized them by BW. N=3 atria were analyzed for each group (*lamp2*$^{e2/e2}$ and their wild-type siblings; no exclusion).

2.5. In vivo echocardiography

We used Vevo 3100 high-frequency imaging system equipped with a 50 MHz linear array transducer (FUJIFILM VisualSonics Inc.). Adult zebrafish were anesthetized by tricaine (0.16 mg/ml) for 5 minutes, placed ventral side up into the sponge. The 50 MHz (MX700) transducer was placed above the zebrafish to provide a sagittal imaging plane of the heart. B-mode images were acquired with an imaging field of view of 9.00 mm in the axial direction and 5.73 mm in the lateral direction, a frame rate of 123 Hz, with medium persistence and a transmit focus at the center of the heart.

2.6. Single cardiomyocyte isolation and morphometry

Single ventricular cardiomyocytes were isolated by enzymatic digestion as previously described [36]. Briefly, excised hearts were perfused with low calcium fish Tyrode solution containing collagenase type II (0.2 mg/ml; Worthington Biochemical Corporation) and trypsin type IX-S (0.12 mg/ml; Sigma) for 15-20 min at 0.5 ml/min flowrate. Cardiomyocytes were photographed in fish using a Tyrode solution in tissue chamber on inverted microscope Nikon Axiovert 135 TV with the help of standard camera. Length and width of the cells were measured using ImageJ software (NIH). Cardiomyocytes (~70) from N=3 hearts from each group were analyzed.

2.7. Single myofibril technique

Single myofibrils were prepared as previously described [36, 37]. Briefly, extracted hearts were washed in phosphate buffered saline, frozen in liquid nitrogen and kept at −80°C. On a day before experiment, hearts were placed to 1% (v/v) Triton in standard relaxing buffer supplemented with protease inhibitors at 4°C overnight. Then, permeabilized zebrafish heart ventricles were homogenized in ice-cold relaxing buffer at 20,000 rpm for 10 s (homogenizer MDT500, 5 mm probe, MicroDisTec, Switzerland). The compositions of bath, relaxing, and activating solutions were as previously described [36]. We selected myofibrils with length of ~50-60 μm and thickness of ~3-5 μm. Exclusion criterion for fibers was rundown of developed tension more than 20% per set of contractions (6-10). All zebrafish single myofibril mechanics experiments were done at 10°C. Details of the protocol can be found in Supplementary Data.

2.8. Statistics

Unpaired two-tailed Student's *t* test was used to compare 2 groups. One-way analysis of variance (ANOVA) was used to detect differences among multiple groups. For survival plots log-rank test was used. In graphs, each value represents the Mean ± S.D. if not otherwise mentioned. *P* values less than 0.05 were considered to be significant.

3. Results

3.1 lamp2$^{e2/e2}$ zebrafish manifest compound phenotypes resembling Danon disease

In the zebrafish, a single *lamp2* gene is found in chromosome 14; it consists of 8 exons (ensemble # ENSDARG00000014914). While exon 1 to 5 in *lamp2,* corresponding to the exons 1-8 in human *LAMP2* [14], are shared among 3 different isoforms, the addition of the exons 6,7, or 8 will result in mRNAs that encode Lamp2b, Lamp2a, and Lamp2c, respectively (Supplementary Fig. 1, B). Zebrafish Lamp2b protein consists of 365 amino acids, which shares 49% identity to the human LAMP2B (Supplementary Fig. 1C).

We generated a *lamp2*$^{e2/e2}$ mutant which has a 5-nt deletion in the exon 2 via TALEN technology (Fig. 1A). The deletion resulted in a shift of the reading frame, presumably truncating all three Lamp2 isoforms (Fig 1A). Hence, the transcript level of *lamp2* was reduced by 90% in the mutant, likely due to non-sense mediated RNA decay (Fig. 1F). Despite our efforts on testing several commercially available antibodies, we did not identify an antibody that recognizes the zebrafish Lamp2 protein, preventing us to assess expressional changes at the protein level. The *lamp2*$^{e2/e2}$ fish were smaller than their wild-type siblings, as indicated by reduced body weight at the ages of 3 months (data not shown) to 9 months (Fig. 1B and C). 74% of the *lamp2*$^{e2/e2}$ fish (14 out of 19 fish, in this clutch) had iris defects, affecting one or both eyes (Supplementary Fig. 2A–C) resembling eye pathology in the Danon disease patients [6]. Compared to their wild-type siblings, *lamp2*$^{e2/e2}$ fish had reduced maximum swimming capacity (U_{crit}) (Fig. 1D). The *lamp2*$^{e2/e2}$ fish started to die at 10 months of age; about 60% of fish survived to 1 year-old (Fig. 1E). Before dying, mutant fish manifested a swirling and turning behavior, prompting neuromuscular defects.

Similar to the Danon disease patients, iPSC models of Danon disease, and the *Lamp2* KO mouse model, we detected elevated levels of p62 and LC3 in fish *lamp2*$^{e2/e2}$ mutants (Fig. 2A, Supplemental Fig. 9B) together with unchanged p62 transcript level (Supplementary Fig. 5D), suggesting severely blocked autophagy in both striated muscles [38]. Blockage of the autophagosomal-lysosomal fusion with bafilomycin A1 further indicated defective autophagy flux in the heart (Fig. 2C, D). An accumulation of characteristic double-membrane autophagic vacuoles with debris had been noted in the perinuclear region of cardiomyocytes on the transmission electron microphotographs in the *lamp2*$^{e2/e2}$ fish at 13 months of age (Fig 2E, F). Together, these data strongly support the *lamp2*$^{e2/e2}$ as a zebrafish Danon disease model.

3.2 lamp2$^{e2/e2}$ zebrafish manifest cardiac remodeling in both chambers

Next, we determined whether the *lamp2*$^{e2/e2}$ hearts manifest HCM-like structural remodeling. We isolated and perfused beating zebrafish hearts on our recently developed Langendorff-like setup under constant flow and collected images of the hearts [32]. Hearts from *lamp2*$^{e2/e2}$ at 10 months of age appeared less transparent than those from their wild-type siblings at diastole (Fig. 3A). The shape of the heart became more round (Fig. 3A), as quantified by increased shape index in mutants (Fig. 3B). To develop a rapid but indirect assay for quantifying thickness of hearts, we measured intensity in the red channel (RCI) of the images of the mutant hearts at diastole and found this index also elevated (Fig. 3C). The absolute sizes of mutant hearts were slightly smaller, although not significantly, as indicated by the end-diastolic volume (EDV; Supplementary Fig. 3A), as well as normalized volumes EDV/BW and ESV/BW at perfusion flowrates from 0.4 to 0.6 ml/min (Supplementary Fig, 3B). We did note significantly increased ESV/BW in mutants at the low perfusion flowrate of 0.05 ml/min (ESV_{05}/BW) (Fig. 3D). Consistent to the transparency and shape data, denser trabeculation of ventricular myocardium in the trichrome-stained heart sections was documented (Fig. 3E, F). In only two hearts obtained from lethargic *lamp2*$^{e2/e2}$ fish (2/26 fish in 1/3 clutch of fish), we noted signs of severe hypertrophic ventricular remodeling with thicker compact layer, as well as fibrosis (Supplementary Fig. 4A, B).

We then employed the Langendorff-like ex vivo heart perfusion system to characterize cardiac pump function in *lamp2*$^{e2/e2}$ [32]. We noted a marginally reduced ejection fraction (EF%), unaffected dynamics of contraction (Supplementary Fig. 3D, E), but significantly reduced fractional area contractility (FAC%) and parameters of strain (RS%, FS%) at perfusion flowrate of 0.4 ml/min (Fig. 3G–I; S3C). We detected significantly diminished expression of ventricular myosin heavy-chain (*vmhc*, 7 out of 7) and activated natriuretic peptide A (*nppa*) in a subset of mutant fish (5 out of 7). two fetal gene molecular markers for cardiac remodeling (Fig. 3J). Other markers of heart failure were not affected (Supplementary Fig, 5). To assess cellular hypertrophy, we isolated individual cardiomyocytes by enzymatic dissociation, but did not detect any differences in their size (Supplementary Fig. 4C, D).

Because patients with Danon disease die from cardiac arrhythmias, we conducted an electrocardiography (ECG) study using the iWorx system (Fig. 4A). We failed to detect any sign of arrhythmia in the *lamp2*$^{e2/e2}$hearts. Instead, we noticed significantly increased amplitudes of P-waves in *lamp2*$^{e2/e2}$ (Fig. 4A and B), suggesting atrial enlargement or hypertrophy [7]. To prevent collapse of atrium, we developed a method to inflate it by retrograde perfusion (Fig. 4C). Indeed, the atrium area in *lamp2*$^{e2/e2}$hearts was almost double its size compared to that in their wild-type siblings (Fig. 4D). Compared to the thin-walled atrium in the wild types, certain areas of the atrium wall in the *lamp2*$^{e2/e2}$ hearts were thicker because of more trabeculated myocardium (Fig. 4E). In summary, we noted signs of hypertrophic remodeling in both cardiac chambers of *lamp2*$^{e2/e2}$.

3.3 Decreased cardiac pump function and blunted β-adrenergic response in the lamp2^{e2,e2} hearts

To confirm cardiac pump function defects, we adopted a non-invasive high frequency echocardiography (HFE) in vivo method (Fig. 5A). We noted significantly decreased ejection fraction (EF), fractional shortening (FS), and fraction area contractility (FAC) in *lamp2*$^{e2/e2}$ hearts (Fig. 5B to D).

Because blunted β-adrenergic response is a common feature of the failing heart in humans [39], we went on to leverage the ex vivo system to analyze effects of isoproterenol. We recently showed that these effects can be reproduced in the zebrafish [32]: injection of a single bolus of isoproterenol into perfusion system induced an immediate increase in EDV and a decrease in ESV in a wild type heart (Fig. 5E, F). We found that the former effect was blunted in *lamp2*$^{e2/e2}$, as indicated by a negative value of ΔEDV, an index reflecting the lusitropic effect (Fig. 5E). By contrast, we did not notice significant changes in ΔESV, an index reflecting the inotropic effect (Fig. 5F). Consistent with ΔEDV, ΔFS and ΔEF also reduced in *lamp2*$^{e2/e2}$ (Fig. 5G; S6A). By contrast, velocities of contraction and relaxation did not differ from their wild-type siblings (Supplementary Fig. 6B, C).

3.4 Increased maximal isometric tension and accelerated activation kinetics in cardiac myofibrils from lamp2$^{e2/e2}$

Prompted by the confirmed cardiac dysfunction in *lamp2*$^{e2/e2}$, we went on to assess kinetics of myofibril activation and relaxation. Single myofibrils with similar cross-sectional area ~10 μm^2 (CSA) were attached to glass micro-probes (Fig. 6A, B). and activation traces from myofibrils were recorded (Fig. 6C). To assess myofibril activation, we quantified the rate of calcium activation (k_{ACT}) when myofibrils were shortening, as well as the rate of force redevelopment (k_{TR}) when a release-re-stretch maneuver was performed 5 seconds after the initial activation (shown with a star '*' in Fig. 6C). Both variables reflect the rate of cross-bridge turnover [40, 41]. To assess myofibril relaxation, we quantified the rates of linear (t_{LIN}. k_{LIN}) and exponential (k_{EXP}) phases of relaxation (Fig. 6C). Both k_{ACT} and k_{TR} were increased in *lamp2*$^{e2/e2}$ myofibrils, indicating faster kinetics of force generation (Fig. 6D and E). By contrast, there were no differences in force-pCa, kinetics of myofibril relaxation as well as in the passive elastic properties of the skinned myocardium (Fig. 6F, H; Supplementary Fig. 9).

We detected increased maximal isometric tension in *lamp2*$^{e2/e2}$ myofibrils, supporting "hypcrcontractility" that might be already suggested by the increased rates k_{ACT} and k_{TR} (Fig, 6D and E). We also noted a diminished Hill coefficient parameter in *lamp2*$^{e2/e2}$ mutants (Fig, 6I). suggesting reduced cooperativity in force generation. Together, our biophysical studies demonstrate that depletion of *lamp2* in zebrafish is able to result in "hypcrcontractility" at the level of a myofibril, a feature that has been reported in both sarcomeric and non-sarcomeric HCM models in mammals [41, 42].

3.5 mTOR inhibition partially rescues cardiac pump function and myofibril contractility defects in lamp2$^{e2/e2}$ hearts

To assess whether mTOR is a therapeutic target for *lamp2*$^{e2/e2}$, we determined the mTOR signaling by western blotting. We noted significantly increased phosphorylation of mTOR and S6 proteins in skeletal muscle, suggesting enhanced mTOR signaling (Fig, 2A, B), However, these two indices were not significantly increased in the heart, despite a tendency of activation. Nevertheless, we bred *mtor*$^{xu015/+}$ into the *lamp2* mutant to generate double mutants. We found that the severely overexpressed LC3-II remained unchanged among the three experimental groups (Supplementary Fig, 9A). suggesting that mTOR inhibition cannot fully repair metabolic abnormality including the defective macroautophagy. We did note that mTOR inhibition was able to attenuate defective autophagic flux (Supplementary Fig, 9C, D). However, accumulation of double-membrane autophagic vacuoles still persisted in the double mutant hearts (Supplementary Fig, 9E, F).

Despite that metabolic abnormality remains in the double mutant, we reasoned that it is still possible that mTOR inhibition alleviate some sequential maladaptive processes triggered by the initial metabolic damage. Indeed, we noted significantly improved EF and FAC in *lamp2*$^{e2/e2}$; mtor^{xu015+} in vivo, while single *mtor*$^{xu015+}$ did not manifest any abnormalities in cardiac contractility (Supplementary Fig, 7), prompting a therapeutic effect of mTOR inhibition on cardiac dysfunction (Fig. 5 B–D). Interestingly, the change in EF can be mainly ascribed to the change in the long axis fractional shortening (FS), but not in the short axis FS (Fig. 5D). Blunted lusitropic effect of isoproterenol was also clearly rescued in *lamp2*$^{e2/e2}$*;mior*$^{xu015/+}$ (Fig. 5E), although mTOR inhibition failed to rescue the blunted ESV and EF change in *lamp2*$^{e2/e2}$, as indexed by ΔEF (Fig. 5F, G). We also did not note any signs of rescue in cardiac morphometric indices including shape, transparency, ESV_{05}/BW, and trabecular fiber thickness (data not shown).

Finally, we tested the rescuing effects of mTOR inhibition at the myofibril level. We found that both rates of force activation, k_{ACT} and km, were effectively rescued in *lamp2*$^{e2/e2}$*:mtor*$^{xu015/+}$. as well as maximal isometric tension (Fig. 6D - G). Intriguingly, in the *lamp2*$^{e2/e2}$*:mior*$^{xu015/+}$ group, myofilament Ca^{2+} sensitivity was reduced (Fig. 6H). However, Hill coefficient was not repaired by mTOR inhibition (Fig. 6I). Together, we concluded that mTOR inhibition is able to at least partially rescue cardiac dysfunction in *lamp2*$^{e2/e2}$, despite the metabolic abnormalities cannot be fully repaired.

4. Discussion

4.1. lamp2$^{e2/e2}$ is a zebrafish model of Danon disease

The genotype of *lamp2*$^{e2/e2}$ was designed to recapitulate representative genetic lesions that cause human Danon disease: most Danon disease-causative mutations are loss-of-function *LAMP2* mutations that resulted in truncation and/or depletion of the encoded LAMP2 protein [4]. Massive accumulation of autophagic vacuoles, likely due to interrupted fusion of autophagosomes with lvsosomes, can be detected in the heart, a characteristic feature of Danon disease [1]. Similar to patients with Danon disease, *lcimp2*^{e2le2} fish show signs of hypertrophic cardiomyopathy, as well as non-cardiac phenotypes that are reminiscent of

human Danon disease, including accumulation of autophagic vacuoles, reduced swimming capacity and iris defects in a portion of the mutant fish.

Despite of similarities, there are notable differences among the zebrafish *lamp2*$^{e2/e2}$, mouse *Lamp2* KO models, and the human Danon disease. In contrast to human X-linked Danon disease, the zebrafish *lamp2* KO is autosomal. Therefore, homozygous *lamp2*$^{e2/e2}$ can recapitulate overall LAMP2 deficiency in human, but not different disease severity between men and women, as noted in humans [5]. Moreover, cardiac phenotypes in humans are very severe [2, 10]. By contrast, the mouse model of Danon disease shows more systemic autophagic lesions: a half of *Lamp 2* deficient mice die shortly after bom likely due to intestinal infarctions/stenosis or pancreatic failure with massive intracellular accumulation of the autophagic vacuoles [15]. In the zebrafish *lamp2*$^{e2/e2}$, cardiac phenotypes are relatively mild: for example, apoptosis was not detected in our fish model with very rare fibrosis, too. Similar to mouse, the *lamp2*$^{e2/e2}$ fish have smaller body size, a phenomenon that has not been reported in humans.

4.2. lamp2$^{e2/e2}$ zebrafish manifest cardiac phenotypes reminiscent of HCM in mammals

We conducted comprehensive studies of the *lamp2*$^{e2/e2}$fish using the newly developed phenotyping tools [32, 36] and noted reduced cardiac pump function and blunted lusitropic β-adrenergic myocardium response. Blunted β-adrenergic response is a common feature of the failing human hearts, which could be due to uncoupling between myofilament Ca^{2+} sensitivity and N-terminal phosphorylation of the cardiac isoform of Troponin I by protein kinase A [43, 44]. It remains to be investigated whether phosphorylation of thin myofilaments is affected in *lamp2* KO upon β-adrenergic stimulation or treatment with protein kinase A in mammalian models. However, the zebrafish may not be the best model to study this because its cardiac Troponin I lacks phosphorylatable N-terminal domain [45].

In mammals, a key phenotypic trait that defines HCM is an increased thickness of the left ventricular wall [2, 8]. However, this index is hard to be measured in a highly trabeculated zebrafish heart. Instead, our studies in *lamp2*$^{e2/e2}$ suggest the following three indices that might define hypertrophic remodeling in adult zebrafish. First, we noted the increased density of the trabecular muscle in the sectioned hearts. We also noted thickened compact layer and fibrosis in a single mutant fish; similar phenotypes have been reported in the rainbow trout hearts upon cold stress [46]. To rapidly measure density or thickness of a zebrafish heart, we developed an indirect index by quantifying Red Channel Intensity of RGB images. Given a zebrafish heart is transparent, we postulated that the appearance of more red pixels on a heart reflects an increased muscle thickness. Second, using the ex vivo Langendorff-like perfusion system, we noted that ESV/BW at low perfusion flowrate was increased. Because at low flowrates the ventricle develops forces against the low pressure, it is likely that systole volume indirectly reflects muscle thickness. However, this hypothesis need to be further tested in the future. Third, at the level of cardiac ventricular myofibrils, we noted the increased maximal isometric tension and accelerated actomyosin activation kinetics, suggesting myofibrillar “hypercontractility”, which have been noted in sarcomeric HCM patients and mammalian models [9, 47–49]. Of note, reduced force of isolated trabeculae has been reported in *Lamp2*-deficient mice [15], which appears in conflict with

our conclusion at the single myofibril level. Because different methods are used, more detailed comparison of sarcomeric contractility changes between fish and mouse models warrants future investigations.

A likely mechanism for the increased kinetics of contraction in *lamp2*$^{e2/e2}$ mutants could be the shift of the prevalent myosin heavy chain isoform in cardiac muscle as a part of the fetal-gene re-programming process. Specifically in *lamp2*$^{e2/e2}$, we noted the reduced expression of *vmhc.* This change in the prevalent myosin heavy chain isoform may affect cross-bridge cycling, maximal isometric tension, relaxation, and energy consumption [50]. Alternatively, the increased maximal isometric tension in *lamp2*$^{e2/e2}$ might be caused by imprecise normalization of force by cross-section area (CSA) of the myofibril due to hypertrophic remodeling. More myofibrils/CSA in *lamp2*$^{e2/e2}$ preparations could result in a bigger tension, if force is normalized by CSA. This possibility could be tested in the future by quantifying myofibril area via the electron microscopy.

In addition to ventricular hypertrophy, we also noted atrial hypertrophy in the *lamp2*$^{e2/e2}$ fish, which is unveiled by the modified ex vivo perfusion system that was originally designed to study ventricular functions. Because enlarged left atrium is frequently found in human heart failure patients [51], this result prompted future studies to determine whether enlarged atrium is a part of pathogenesis in patients with Danon disease.

4.3 mTOR inhibition partially attenuates cardiac defects in lamp2 KO fish

Unlike the cell culture models that can only be used to study primary defects, in vivo animal models of cardiomyopathy are able to identify therapeutic strategies that affect both primary and secondary phenotypes. Here, we report therapeutic effects of mTOR inhibition in cardiac contractility defects in *lamp2*$^{e2/e2}$ fish. Comprehensive phenotyping of *lamp2*$^{e2/e2}$ indicated that part of cardiac phenotypes, including blunted lusitropic β-adrenergic response, maximal isometric tension, and actomyosin activation kinetics can be rescued by mTOR inhibition. Interestingly, mTOR inhibition has been found to be effective in reversing cardiac hypercontractility in the Noonan syndrome, a non-sarcomeric HCM that is incurred by *Shp2* mutations [20, 21, 52]. Together, these data suggest that HCM of different etiology might converge on a final common pathway that is characterized by sarcomere hypercontractility, while mTOR inhibition is effective in attenuating this critical step of pathogenesis. Mechanistically, we show that mTOR inhibition is able to partially repair the primary metabolic abnormalities such as autophagic flux. However, severe autophagic defects as indicated by the increased LC3 expression and accumulated autophagic vacuoles still persist in double mutants. Therefore, we favor the hypothesis that mTOR exerts its therapeutic effects via attenuating key sequential cascade events such as those driving the switch of the pathogenesis from the compensational to the decompensational phase.

The present study highlighted both strength and limitation of the zebrafish model. Empowered by the emerging phenotyping tools, zebrafish are highly efficient for longitudinally genetic studies, but are difficult for signaling pathway analysis. How mTOR inhibition affects metabolic abnormalities in Danon disease remains enigmatic, which warrants further investigation. We recommend using the cell culture platform for this type of studies, while zebrafish shall be used to decipher sequential cascade events that cannot be

modeled in the cell culture models. Capitalized on the efficient zebrafish forward genetics, a unique future research direction enabled by the zebrafish model is to identify additional therapeutic strategies for the Danon disease model by systematically discovering genetic modifiers [24, 25, 29, 30].

5. Conclusions

Through comprehensive cardiac phenotyping, we established *lamp2*$^{e2/e2}$ as the first adult zebrafish model of HCM in Danon disease. While we previously showed the feasibility of using acquired adult zebrafish models to assess therapeutic strategies [24, 25, 29], here, we further demonstrated that the therapeutic effects of mTOR inhibition can be extended to the *lamp2*$^{e2/e2}$ cardiomyopathy model.

Supplementary Material

Refer to Web version on PubMed Central for supplementary material.

Acknowledgements

We thank Kashia Stragey and Beninio Gore for the fish husbandry; we also thank Dr. Matthew Lowerison for the help with the ultrasound scanner.

Sources of funding

The work was supported by NIH R01HL107304, HL81753, HL111437 and Mayo Foundation to X.X.

References

[1]. Roos JCP, Daniels MJ, Morris E, Hyry HI, Cox TM, Heterogeneity in a large pedigree with Danon disease: Implications for pathogenesis and management, Mol Genet Metab 123(2) (2018) 177–183. [PubMed: 28822614]

[2]. Maron BJ, Roberts WC, Arad M, Haas TS, Spirito P, Wright GB, Almquist AK, Baffa JM, Saul JP, Ho CY, Seidman J, Seidman CE, Clinical outcome and phenotypic expression in LAMP2 cardiomyopathy, JAMA 301(12) (2009) 1253–9. [PubMed: 19318653]

[3]. Danon MJ, Oh SJ, DiMauro S, Manaligod JR, Eastwood A, Naidu S, Schliselfeld LH, Lysosomal glycogen storage disease with normal acid maltase, Neurology 31(1) (1981) 51–7. [PubMed: 6450334]

[4]. D'Souza R S, Levandowski C, Slavov D, Graw SL, Allen LA, Adler E, Mestroni L, Taylor MR, Danon disease: clinical features, evaluation, and management, Circ Heart Fail 7(5) (2014) 843–9. [PubMed: 25228319]

[5]. Endo Y, Furuta A, Nishino I, Danon disease: a phenotypic expression of LAMP-2 deficiency, Acta Neuropathol 129(3) (2015) 391–8. [PubMed: 25589223]

[6]. Prall FR, Drack A, Taylor M, Ku L, Olson JL, Gregory D, Mestroni L, Mandava N, Ophthalmic manifestations of Danon disease, Ophthalmology 113(6) (2006) 1010–3. [PubMed: 16751040]

[7]. Fuster V, Harrington RA, Narula J, Eapen ZJ, Hurst's the heart, Fourteenth edition ed., McGraw-Hill Education, New York, 2017.

[8]. Ahmad F, Seidman JG, Seidman CE, The genetic basis for cardiac remodeling, Annu Rev Genomics Hum Genet 6 (2005) 185–216. [PubMed: 16124859]

[9]. Green EM, Wakimoto H, Anderson RL, Evanchik MJ, Gorham JM, Harrison BC, Henze M, Kawas R, Oslob JD, Rodriguez HM, Song Y, Wan W, Leinwand LA, Spudich JA, McDowell RS, Seidman JG, Seidman CE, A small-molecule inhibitor of sarcomere contractility suppresses hypertrophic cardiomyopathy in mice, Science 351(6273) (2016) 617–21. [PubMed: 26912705]

[10]. Nascimbeni AC, Fanin M, Angelini C, Sandri M, Autophagy dysregulation in Danon disease, Cell Death Dis 8(1) (2017) e2565.

[11]. Chi C, Leonard A, Knight WE, Beussman KM, Zhao Y, Cao Y, Londono P, Aune E, Trembley MA, Small EM, Jeong MY, Walker LA, Xu H, Sniadecki NJ, Taylor MR, Buttrick PM, Song K, LAMP-2B regulates human cardiomyocyte function by mediating autophagosome-lysosome fusion, Proc Natl Acad Sci U S A 116(2) (2019) 556–565. [PubMed: 30584088]

[12]. Fujiwara Y, Hase K, Wada K, Kabuta T, An RNautophagy/DNautophagy receptor, LAMP2C, possesses an arginine-rich motif that mediates RNA/DNA-binding, Biochem Biophys Res Commun 460(2) (2015) 281–6. [PubMed: 25772617]

[13]. Nishino I, Fu J, Tanji K, Yamada T, Shimojo S, Koori T, Mora M, Riggs JE, Oh SJ, Koga Y, Sue CM, Yamamoto A, Murakami N, Shanske S, Byrne E, Bonilla E, Nonaka I, DiMauro S, Hirano M, Primary LAMP-2 deficiency causes X-linked vacuolar cardiomyopathy and myopathy (Danon disease), Nature 406(6798) (2000) 906–10. [PubMed: 10972294]

[14]. Konecki D, An alternative spliced form of the human lysosome-associated membrane protein-2 gene is expressed in a tissue-specific manner, Biochemical and Biophysical research communication (1995).

[15]. Tanaka Y, Guhde G, Suter A, Eskelinen EL, Hartmann D, Lullmann-Rauch R, Janssen PM, Blanz J, von Figura K, Saftig P, Accumulation of autophagic vacuoles and cardiomyopathy in LAMP-2-deficient mice, Nature 406(6798) (2000) 902–6. [PubMed: 10972293]

[16]. Hashem SI, Murphy AN, Divakaruni AS, Klos ML, Nelson BC, Gault EC, Rowland TJ, Perry CN, Gu Y, Dalton ND, Bradford WH, Devaney EJ, Peterson KL, Jones KL, Taylor MRG, Chen J, Chi NC, Adler ED, Impaired mitophagy facilitates mitochondrial damage in Danon disease, J Mol Cell Cardiol 108 (2017) 86–94. [PubMed: 28526246]

[17]. Korolchuk VI, Saiki S, Lichtenberg M, Siddiqi FH, Roberts EA, Imarisio S, Jahreiss L, Sarkar S, Futter M, Menzies FM, O'Kane CJ, Deretic V, Rubinsztein DC, Lysosomal positioning coordinates cellular nutrient responses, Nat Cell Biol 13(4) (2011) 453–60. [PubMed: 21394080]

[18]. Kim YM, Jung CH, Seo M, Kim EK, Park JM, Bae SS, Kim DH, mTORC1 phosphorylates UVRAG to negatively regulate autophagosome and endosome maturation, Mol Cell 57(2) (2015) 207–18. [PubMed: 25533187]

[19]. Narita M, Young AR, Arakawa S, Samarajiwa SA, Nakashima T, Yoshida S, Hong S, Berry LS, Reichelt S, Ferreira M, Tavare S, Inoki K, Shimizu S, Narita M, Spatial coupling of mTOR and autophagy augments secretory phenotypes, Science 332(6032) (2011) 966–70. [PubMed: 21512002]

[20]. Marin TM, Keith K, Davies B, Conner DA, Guha P, Kalaitzidis D, Wu X, Lauriol J, Wang B, Bauer M, Bronson R, Franchini KG, Neel BG, Kontaridis MI, Rapamycin reverses hypertrophic cardiomyopathy in a mouse model of LEOPARD syndrome-associated PTPN11 mutation, J Clin Invest 121(3) (2011) 1026–43. [PubMed: 21339643]

[21]. Sciarretta S, Forte M, Frati G, Sadoshima J, New Insights Into the Role of mTOR Signaling in the Cardiovascular System, Circ Res 122(3) (2018) 489–505. [PubMed: 29420210]

[22]. Dvornikov AV, de Tombe PP, Xu X, Phenotyping cardiomyopathy in adult zebrafish, Prog Biophys Mol Biol 138 (2018) 116–125. [PubMed: 29884423]

[23]. Shih YH, Zhang Y, Ding Y, Ross CA, Li H, Olson TM, Xu X, Cardiac transcriptome and dilated cardiomyopathy genes in zebrafish, Circ Cardiovasc Genet 8(2) (2015) 261–9. [PubMed: 25583992]

[24]. Ding Y, Sun X, Xu X, TOR-autophagy signaling in adult zebrafish models of cardiomyopathy, Autophagy 8(1) (2012) 142–3. [PubMed: 22186229]

[25]. Ding Y, Long PA, Bos JM, Shih YH, Ma X, Sundsbak RS, Chen J, Jiang Y, Zhao L, Hu X, Wang J, Shi Y, Ackerman MJ, Lin X, Ekker SC, Redfield MM, Olson TM, Xu X, A modifier screen identifies DNAJB6 as a cardiomyopathy susceptibility gene, JCI Insight 1(14) (2016).

[26]. Packard RRS, Baek KI, Beebe T, Jen N, Ding Y, Shi F, Fei P, Kang BJ, Chen PH, Gau J, Chen M, Tang JY, Shih YH, Ding Y, Li D, Xu X, Hsiai TK, Automated Segmentation of Light-Sheet Fluorescent Imaging to Characterize Experimental Doxorubicin-Induced Cardiac Injury and Repair, Sci Rep 7(1) (2017) 8603. [PubMed: 28819303]

[27]. Sun X, Hoage T, Bai P, Ding Y, Chen Z, Zhang R, Huang W, Jahangir A, Paw B, Li YG, Xu X, Cardiac hypertrophy involves both myocyte hypertrophy and hyperplasia in anemic zebrafish, PLoS One 4(8) (2009) e6596. [PubMed: 19672293]

[28]. Kossack M, Hein S, Juergensen L, Siragusa M, Benz A, Katus HA, Most P, Hassel D, Induction of cardiac dysfunction in developing and adult zebrafish by chronic isoproterenol stimulation, J Mol Cell Cardiol 108 (2017) 95–105. [PubMed: 28554511]

[29]. Ding Y, Sun X, Redfield M, Kushwaha S, Xu X, Target of rapamcyin (TOR)-based therapeutics for cardiomyopathy: insights from zebrafish genetics, Cell Cycle 11(3) (2012) 428–9. [PubMed: 22262179]

[30]. Ding Y, Sun X, Huang W, Hoage T, Redfield M, Kushwaha S, Sivasubbu S, Lin X, Ekker S, Xu X, Haploinsufficiency of target of rapamycin attenuates cardiomyopathies in adult zebrafish, Circ Res 109(6) (2011) 658–69. [PubMed: 21757652]

[31]. Wang LW, Huttner IG, Santiago CF, Kesteven SH, Yu ZY, Feneley MP, Fatkin D, Standardized echocardiographic assessment of cardiac function in normal adult zebrafish and heart disease models, Dis Model Mech 10(1) (2017) 63–76. [PubMed: 28067629]

[32]. Dvornikov AV, Zhang H, Huttner IG, Ma X, Santiago CF, Fatkin D, Xu X, A Langendorff-like system to quantify cardiac pump function in adult zebrafish, Dis Model Mech (2018).

[33]. Cao H, Yu F, Zhao Y, Zhang X, Tai J, Lee J, Darehzereshki A, Bersohn M, Lien C-L, Chi NC, Wearable multi-channel microelectrode membranes for elucidating electrophysiological phenotypes of injured myocardium, Integrative Biology 6(8) (2014) 789–795. [PubMed: 24945366]

[34]. Cao J, Poss KD, Explant culture of adult zebrafish hearts for epicardial regeneration studies, Nat Protoc 11(5) (2016) 872–81. [PubMed: 27055096]

[35]. Le T, Lenning M, Clark I, Bhimani I, Fortunato J, Marsh P, Xu X, Cao H, Acquisition, Processing and Analysis of Electrocardiogram in Awake Zebrafish, IEEE Sensors (2019).

[36]. Dvornikov AV, Dewan S, Alekhina OV, Pickett FB, de Tombe PP, Novel approaches to determine contractile function of the isolated adult zebrafish ventricular cardiac myocyte, Journal of Physiology-London 592(9) (2014) 1949–1956.

[37]. de Tombe PP, Stienen GJ, Impact of temperature on cross-bridge cycling kinetics in rat myocardium, J Physiol 584(Pt 2) (2007) 591–600. [PubMed: 17717017]

[38]. Tanida I, Ueno T, Kominami E, LC3 and Autophagy, Methods Mol Biol 445 (2008) 77–88. [PubMed: 18425443]

[39]. Wilkinson R, Song W, Smoktunowicz N, Marston S, A dilated cardiomyopathy mutation blunts adrenergic response and induces contractile dysfunction under chronic angiotensin II stress, Am J Physiol Heart Circ Physiol 309(11) (2015) H1936–46. [PubMed: 26432839]

[40]. Brenner B, Effect of Ca2+ on cross-bridge turnover kinetics in skinned single rabbit psoas fibers: implications for regulation of muscle contraction, Proc Natl Acad Sci U S A 85(9) (1988) 3265–9. [PubMed: 2966401]

[41]. Belus A, Piroddi N, Scellini B, Tesi C, D'Amati G, Girolami F, Yacoub M, Cecchi F, Olivotto I, Poggesi C, The familial hypertrophic cardiomyopathy-associated myosin mutation R403Q accelerates tension generation and relaxation of human cardiac myofibrils, J Physiol 586(15) (2008) 3639–44. [PubMed: 18565996]

[42]. Clay SA, Domeier TL, Hanft LM, McDonald KS, Krenz M, Elevated Ca2+ transients and increased myofibrillar power generation cause cardiac hypercontractility in a model of Noonan syndrome with multiple lentigines, Am J Physiol Heart Circ Physiol 308(9) (2015) H1086–95. [PubMed: 25724491]

[43]. Messer AE, Marston SB, Investigating the role of uncoupling of troponin I phosphorylation from changes in myofibrillar Ca(2+)-sensitivity in the pathogenesis of cardiomyopathy, Front Physiol 5 (2014) 315. [PubMed: 25202278]

[44]. Saad NS, Elnakish MT, Ahmed AAE, Janssen PML, Protein Kinase A as a Promising Target for Heart Failure Drug Development, Arch Med Res (2019).

[45]. Fu CY, Lee HC, Tsai HJ, The molecular structures and expression patterns of zebrafish troponin I genes, Gene Expr Patterns 9(5) (2009) 348–56. [PubMed: 19602390]

[46]. Keen AN, Fenna AJ, McConnell JC, Sherratt MJ, Gardner P, Shiels HA, The Dynamic Nature of Hypertrophic and Fibrotic Remodeling of the Fish Ventricle, Front Physiol 6 (2015) 427. [PubMed: 26834645]

[47]. Davis J, Davis LC, Correll RN, Makarewich CA, Schwanekamp JA, Moussavi-Harami F, Wang D, York AJ, Wu H, Houser SR, Seidman CE, Seidman JG, Regnier M, Metzger JM, Wu JC, Molkentin JD, A Tension-Based Model Distinguishes Hypertrophic versus Dilated Cardiomyopathy, Cell 165(5) (2016) 1147–1159. [PubMed: 27114035]

[48]. Debold EP, Schmitt JP, Patlak JB, Beck SE, Moore JR, Seidman JG, Seidman C, Warshaw DM, Hypertrophic and dilated cardiomyopathy mutations differentially affect the molecular force generation of mouse alpha-cardiac myosin in the laser trap assay, Am J Physiol Heart Circ Physiol 293(1) (2007) H284–91. [PubMed: 17351073]

[49]. Adhikari AS, Kooiker KB, Sarkar SS, Liu C, Bernstein D, Spudich JA, Ruppel KM, Early-Onset Hypertrophic Cardiomyopathy Mutations Significantly Increase the Velocity, Force, and Actin-Activated ATPase Activity of Human beta-Cardiac Myosin, Cell Rep 17(11) (2016) 2857–2864. [PubMed: 27974200]

[50]. Racca AW, Klaiman JM, Pioner JM, Cheng Y, Beck AE, Moussavi-Harami F, Bamshad MJ, Regnier M, Contractile properties of developing human fetal cardiac muscle, J Physiol 594(2) (2016) 437–52. [PubMed: 26460603]

[51]. Patel DA, Lavie CJ, Milani RV, Shah S, Gilliland Y, Clinical implications of left atrial enlargement: a review, Ochsner J 9(4) (2009) 191–6. [PubMed: 21603443]

[52]. Schramm C, Fine DM, Edwards MA, Reeb AN, Krenz M, The PTPN11 loss-of-function mutation Q510E-Shp2 causes hypertrophic cardiomyopathy by dysregulating mTOR signaling, Am J Physiol Heart Circ Physiol 302(1) (2012) H231–43. [PubMed: 22058153]

Highlights

- Zebrafish has a single *LAMP2* homologue
- Loss-of-funotion of *lamp2* in zebrafish models human Danon disease
- Both metabolic abnormality and cardiac dysfunction are recapitulated
- *mtor* inhibition attenuates cardiac dysfunction while metabolic abnormality persists

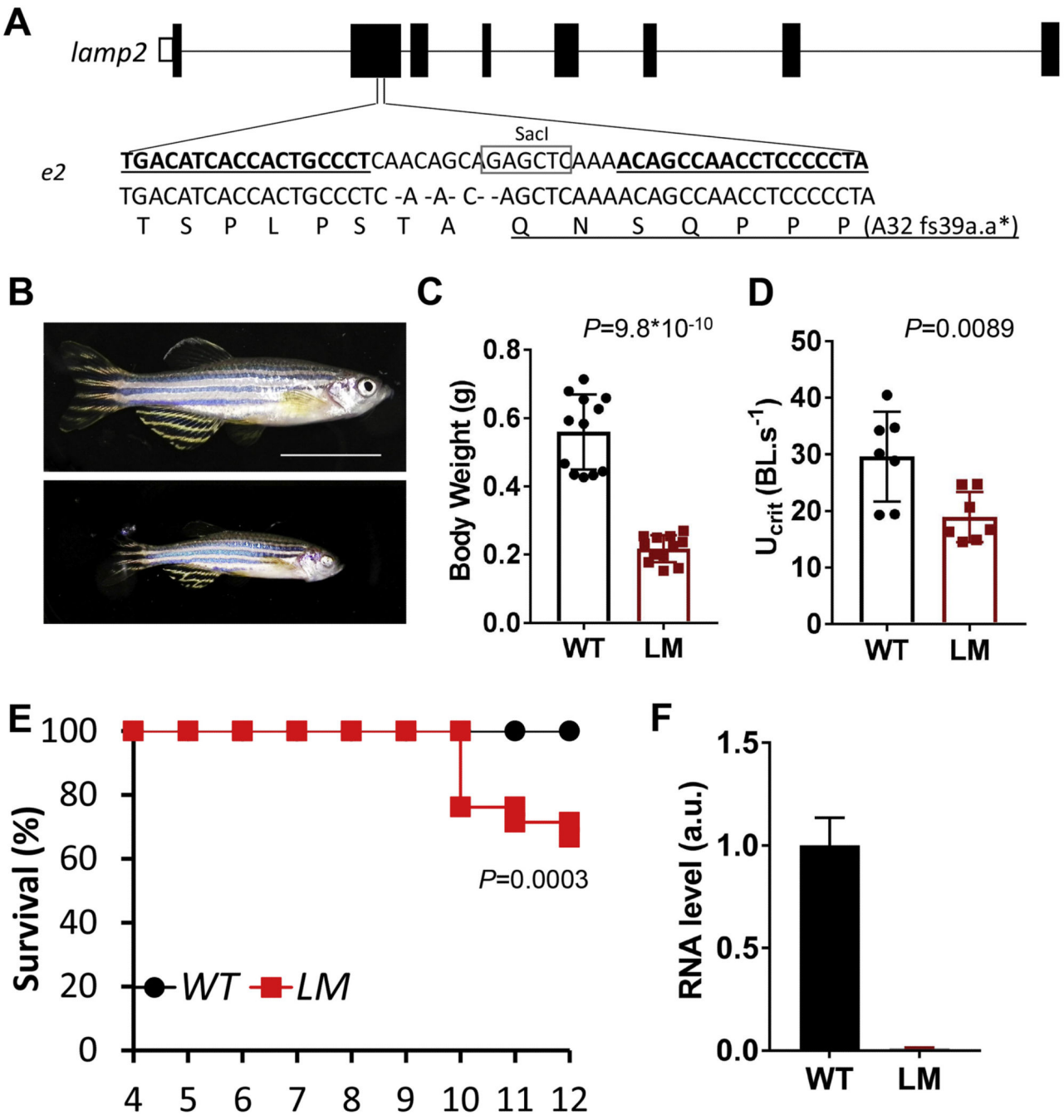

Fig. 1. Generation of *lamp2*$^{e2/e2}$.

A. 5-nt deletion in the 2nd exon of *lamp2* gene results in premature stop codon. Sequences targeted by TALEN are underlined. SacI recognition site is boxed, which was used for genotyping. B. Representative images of wild-type (WT) and *lamp2*$^{e2/e2}$ (LM) fish at 9 months of age. Scale bar is 1 cm. C. Body weight is reduced in *lamp2*$^{e2/e2}$ fish (N=12). D. Swimming capacity (U_{cri}) is decreased in *lamp2*$^{e2/e2}$ fish (N=7). E. Survival plot (N=21). F. *lamp2* transcript is effectively depleted, as shown by qRT-PCR (N=3).

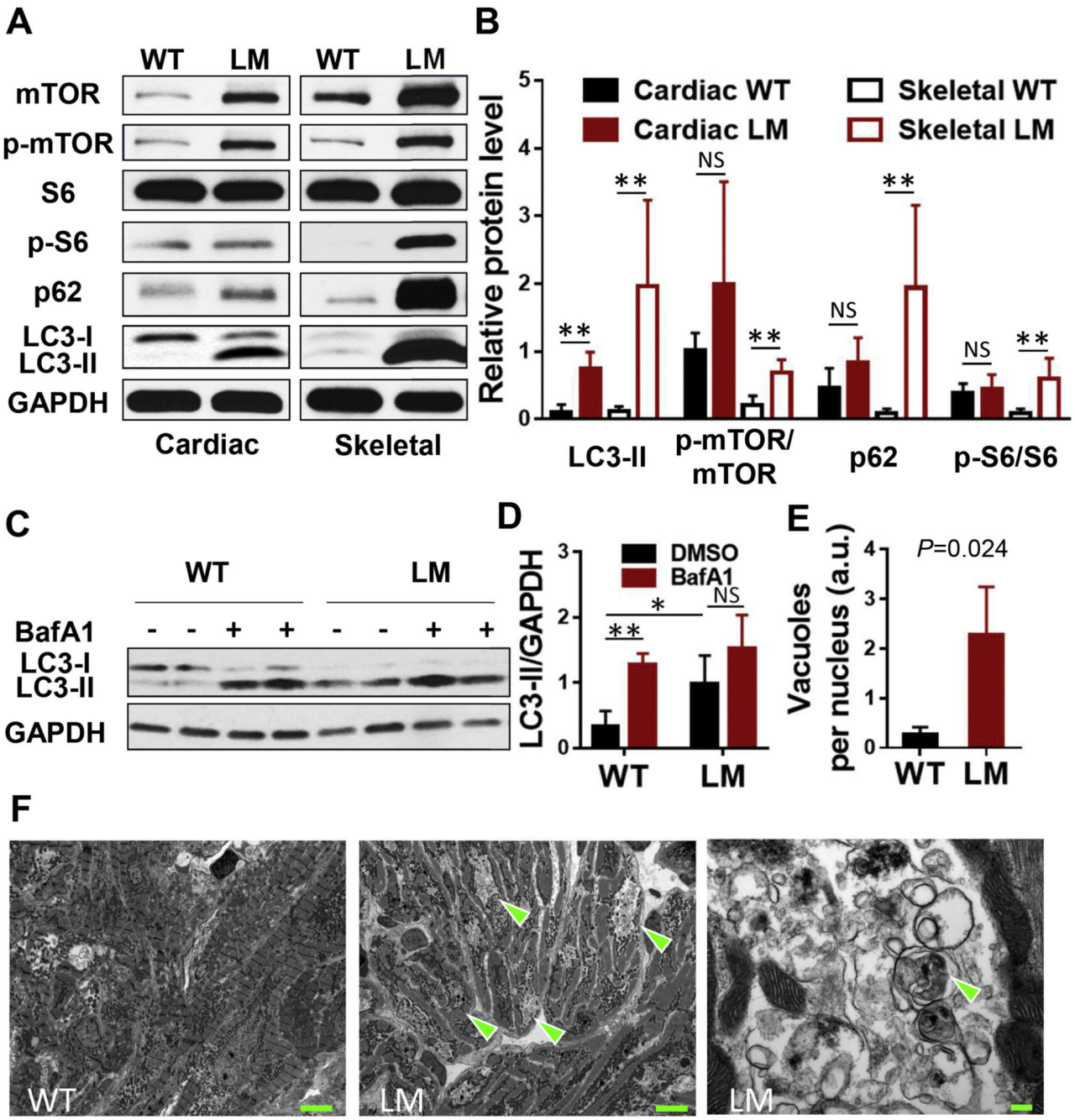

Fig. 2. Metabolic abnormalities in *lamp2*$^{e2/e2}$.

A, B. Shown are western blots of the cardiac and skeletal muscle protein extracts suggesting increased mTOR signaling and aberrant autophagv in *lamp2*$^{e2/e2}$ (Cardiac: N=4; Skeletal: N=5). C, D. Myocardium tissue from lamp2 mutants had higher basal level of LC3-II, and failed to further increase the level of LC3-II upon bafilomycin Al treatment (N=5). E. Quantification of autophagic vacuoles (N=3 hearts each). P<0.05 with WT, F. Representative TEM photographs of cardiac ultra-thin slices (13 months of age). Arrowheads indicate aggregations of autophagic vacuoles in *lamp2*$^{e2/e2}$. At right panel, higher magnification

revealed autophagosomes surrounded by double membranes. Scale bars: 5 μm (left and middle panel) and 200 nm (right panel). * $P<0.05$, ** $P<0.01$.

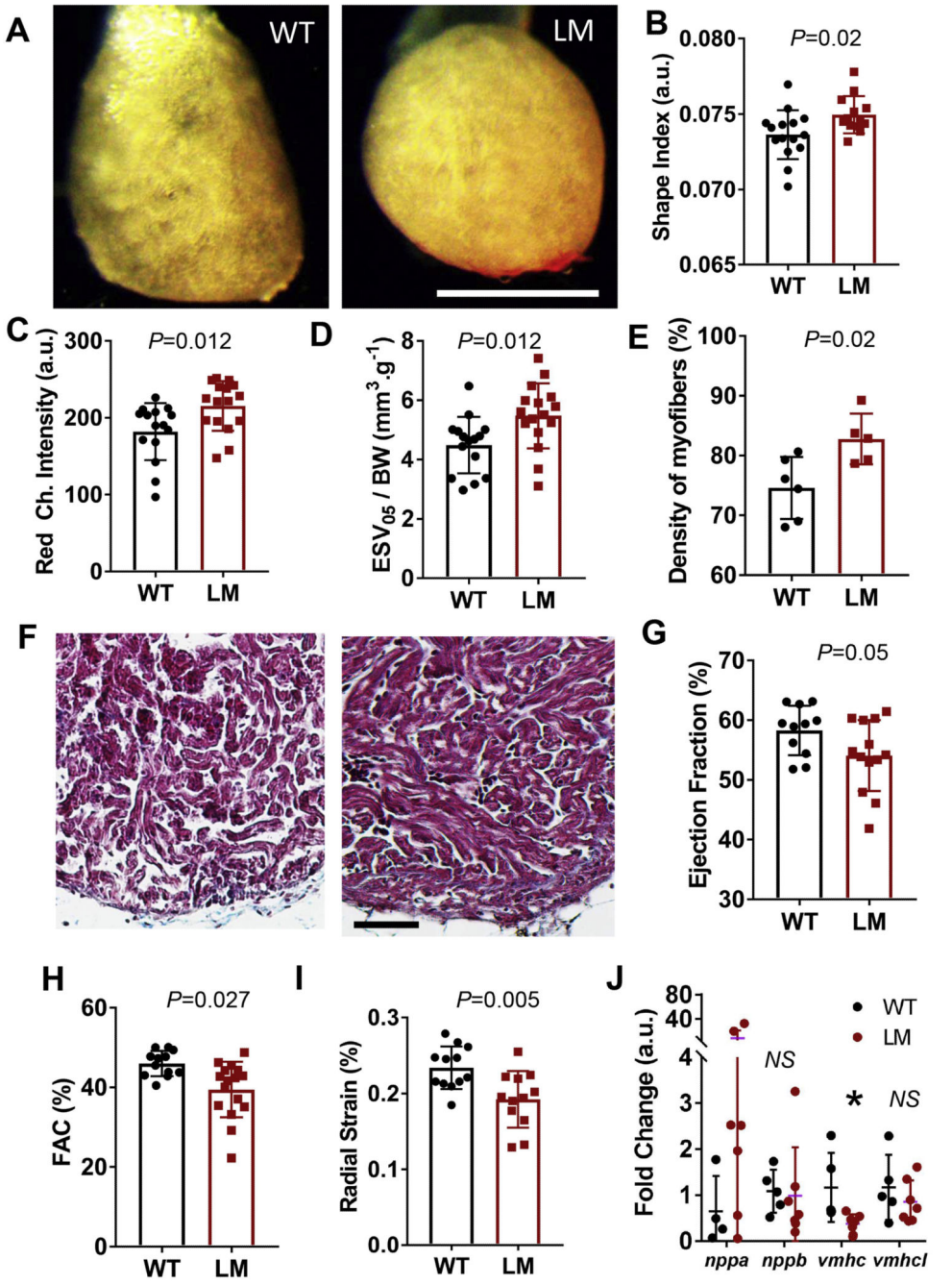

Fig. 3. Ventricular remodeling in *lamp2*$^{e2/e2}$ hearts.

A. Images of isolated ex vivo perfused hearts. Ventricles in *lamp2*$^{e2/e2}$ appear rounder. Scale bar is 1 mm. **B.** Shape index (area over perimeter squared) is increased in *lamp2*$^{e2/e2}$ fish (N=15 for wild-type and 16 for *lamp2*$^{e2/e2}$). C. Red channel intensity is bigger in *lamp2*$^{e2/e2}$ hearts, supporting denser tissue (N=15 for wild-type and 16 for *lamp2*$^{e2/e2}$). D. Increased end-systolic volume at low flow (0.05 ml/min; ESV_{05}) in *lamp2*$^{e2/e2}$hearts (N=15 for wild-tvpe and 16 for *lamp2*$^{e2/e2}$). E. Quantification of F (N=6 hearts for wild-type and N=5 for *lamp2*$^{e2/e2}$). F. Trichrome-stained heart slices show denser trabeculae myocardium. Scale bar

is 50 μm. G. Reduced ejection fraction (EF%), H. Reduced fractional area contractility (FAC %), and I. reduced radial strain both suggest compromised cardiac pump function in *lamp2*$^{e2/e2}$ (LM). Shown in G-I are ex vivo studies of Langendorff-like perfused hearts (N=12). J. qRT-PCR to quantify transcripts of fetal gene program (N=5 and 7 for WT and LM, respectively). *P<0.05.

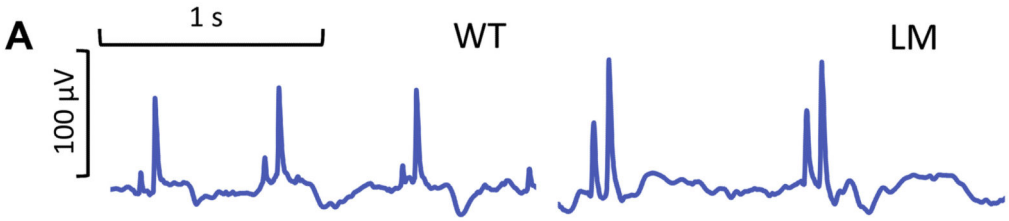

B

	lamp2 $^{+/+}$	*lamp2* $^{e2/e2}$
Fish number	11	14
QTc interval (ms)	328 ± 40	324 ± 34
Heart Rate (bpm)	119 ± 43	111 ± 39
R wave (μV)	52.5 ± 33	75.98 ± 26
P wave (μV)	10.1 ± 4.5	29.4 ± 18 *

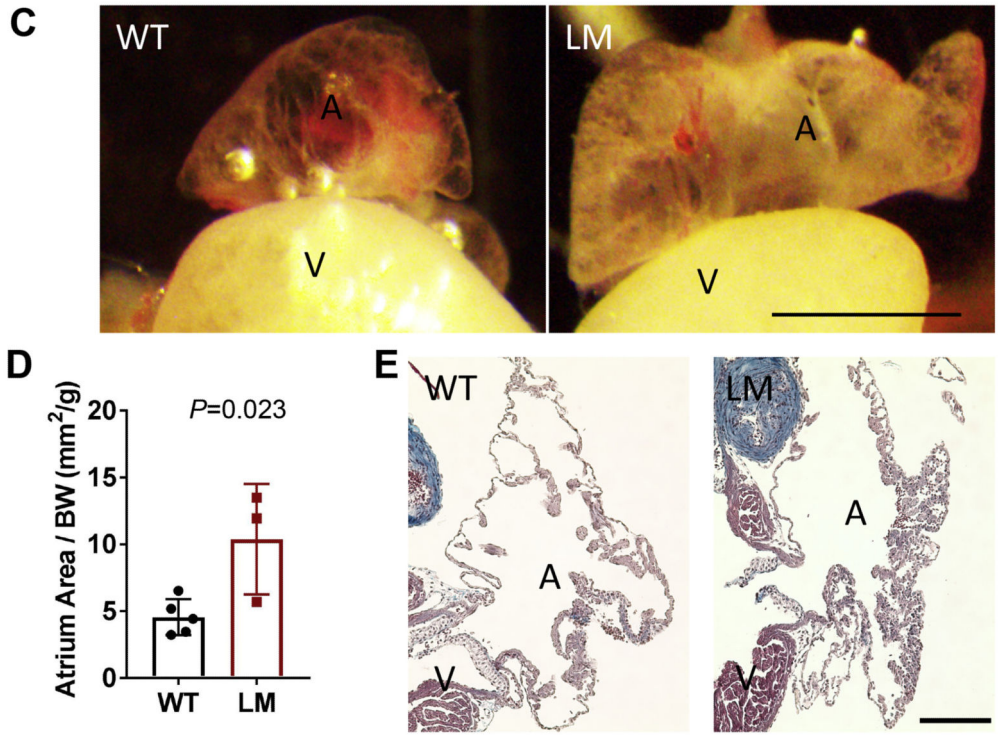

Fig. 4. Atrial hypertrophy in *lamp2*$^{e2/e2}$.

A. Representative electrocardiograms. Note increased magnitudes of P-waves in *lamp2*$^{e2/e2}$(LM, right panel). B. Quantification of ECG parameters: P-wave magnitude is increased (*P<0.0005.). C. Representative images of the inflated atrium. Atria in *lamp2*$^{e2/e2}$ appear bigger and less transparent. Scale bar is 0.8 mm. D. Quantification of the area of atria averaged from two perpendicular planes and normalized by BW (N=3). E. Trichrome staining of the atrial slices. Additional trabeculae were noted in atria of *lamp2*$^{e2/e2}$. Scale bar is 100 um.

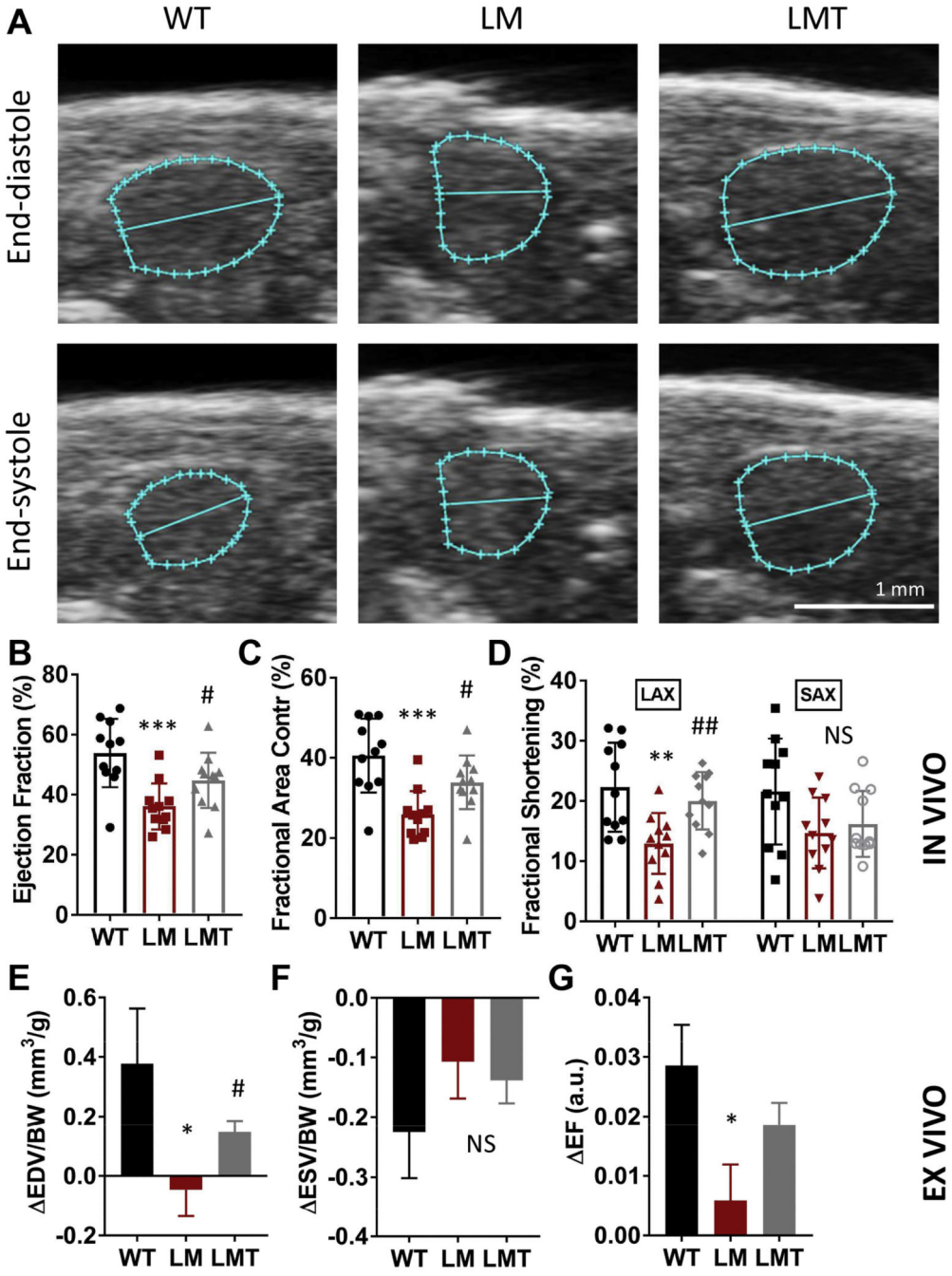

Fig. 5. mTOR inhibition alleviates cardiac dysfunction and blunted β-adrenergic response in *lamp2*$^{e2/e2}$.

A. Representative end-diastolic and end-systolic images of ventricles from echocardiography. B-D. In vivo parameters of cardiac pump function via HFE (N=11 for all groups). Both ejection fraction (EF%) and fractional area contractility (FAC%) were reduced in *lamp2*$^{e2/e2}$ (LM), and were partially rescued in *lamp2*$^{e2/e2}$; *xu015*$^{+/-}$ (LMT). Fractional shortening (FS%) at the long axis (LAX), but not short axis (SAX), was rescued. E-G. Ex vivo indices of the response to isoproterenol (N=15 for the wild-type, 16 for *lamp2*$^{e2/e2}$, and 11 for *lamp2*$^{e2/e2}$; *xu015*$^{+/-}$). The ISO-induced increase of EDV (ΔEDV) and EF (ΔEF)

were blunted in LM, but rescued in LMT group. By contrast, the ISO-induced increase in ESV (ΔESV) was not affected. (Mean ± SEM in the ex vivo ISO response experiment). * $P < 0.05$, LM to WT, # $P < 0.05$, LMT to LM group (rescue).

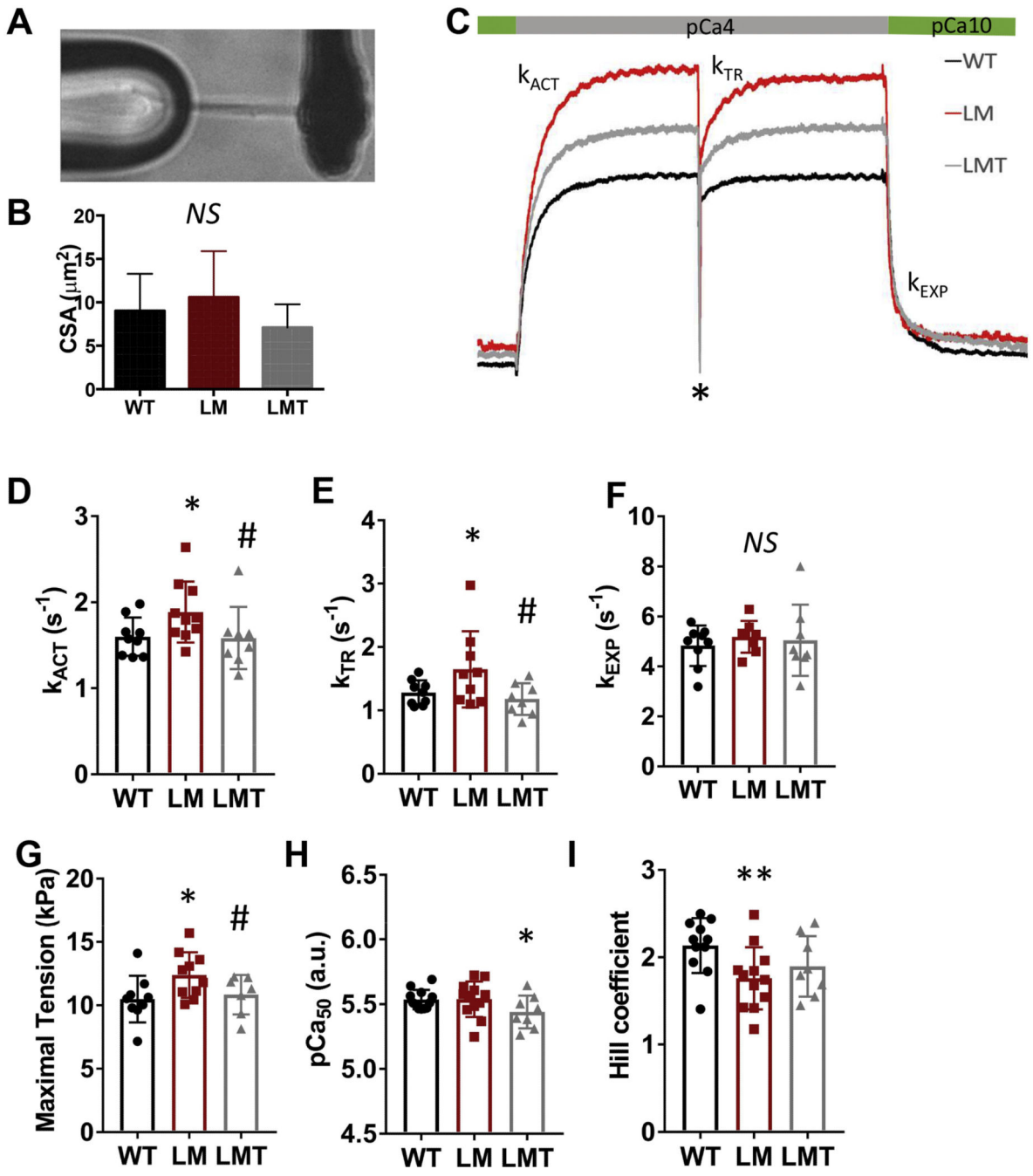

Fig. 6. mTOR inhibition normalizes maximal isometric tension and kinetics of activation in single myofibrils.

A. A representative image of a single myofibril preparation attached to the glass micro-tools. B. Cross-sectional area (CSA) of myofibrils in experiments (N=9. 10 and 8 for the wild-type, *lamp2*$^{e2/e2}$, and *lamp2*$^{e2/e2}$; *xu015*$^{+/-}$, respectively). C. Schematics of the calcium activation and force re-development traces in single myofibrils during release-re-stretch maneuver (*). Shown are WT, LM and LMT groups; D and E. Rates of calcium activation (k_{ACT}) and force re-development (k_{TR}) are both higher in *lamp2*$^{e2/e2}$ (LM) and normalized in double mutant (LMT). F. Parameters of the rate of fast exponential relaxation (k_{EXP}) have

no difference among three groups. G. Maximal tension is increased in *lamp2*$^{e2/e2}$ (LM), but rescued in *lamp2*$^{e2/e2}$; *xu015*$^{+/-}$ (LMT). H. Calcium sensitivity (pCa_{50}) is reduced only in double mutant (LMT). I. Hill coefficient is decreased in both LM and LMT groups. * - $p < 0.05$ to WT # - $p<0.05$ to LM group (rescue).